Relationships between spectral optical properties and optically active substances in a clear oligotrophic lake

Claude Belzile,[1,2] Warwick F. Vincent,[3] Clive Howard-Williams,[4] Ian Hawes,[5] Mark R. James,[5] Michio Kumagai,[6] and Collin S. Roesler[1]

Received 9 February 2004; revised 10 September 2004; accepted 13 October 2004; published 18 December 2004.

[1] The absorption and scattering coefficients in the euphotic zone of oligotrophic Lake Taupo, New Zealand, were measured at 19 stations across the 620 km^2 lake in late fall during the period of mixed layer deepening and development of the annual phytoplankton maximum. These coefficients were subsequently related to the water content of colored dissolved organic matter (CDOM), phytoplankton, and nonalgal particles via measurements of the absorption spectra of these optically active substances and of chlorophyll *a* and suspended particle concentrations. Measurements of the spectral diffuse attenuation coefficient for downwelling irradiance (K_d) and of reflectance (L_u/E_d) revealed that the clear blue waters of Lake Taupo had a minimum K_d of 0.09 m^{-1} at 500 nm and maximum reflectance at 490 nm. The measured K_d and L_u/E_d were well described by modeled spectra that were computed using a radiative transfer model (Hydrolight) assuming relatively low values for the backscattering ratio (0.008–0.014). The relationships established here between the optical properties and optically active substances were consistent with previous observations in case 2 marine waters, and they will provide a basis for prediction of eutrophication, climate, and other environmental effects on the blueness and transparency of large oligotrophic lakes. *INDEX TERMS:* 4847 Oceanography: Biological and Chemical: Optics; 1803 Hydrology: Anthropogenic effects; 1871 Hydrology: Surface water quality; 1845 Hydrology: Limnology; *KEYWORDS:* oligotrophic lake, optics

Citation: Belzile, C., W. F. Vincent, C. Howard-Williams, I. Hawes, M. R. James, M. Kumagai, and C. S. Roesler (2004), Relationships between spectral optical properties and optically active substances in a clear oligotrophic lake, *Water Resour. Res.*, *40*, W12512, doi:10.1029/2004WR003090.

1. Introduction

[2] The optical properties of lakes have a strong influence on the public awareness of environmental change as losses of water clarity or changing color are among the first indicators of declining water quality. Optical properties also play a major role in the ecological structure and functioning of lakes. Solar energy penetration largely determines the biological productivity of aquatic ecosystems by controlling the heat budget, light availability for autotrophs at the base of the food web, and exposure to photoreactive ultraviolet (UV) radiation. The optical properties of lakes are likely to be highly sensitive to global changes such as climate warming and stratospheric ozone depletion [*Schindler et al.*, 1990; *Vincent et al.*, 1998] as well as to local changes in land use such as deforestation and farming [*Goldman*, 1988; *Seehausen et al.*, 1997; *Rae et al.*, 2001], and they provide an integrated index of these combined effects [*Kumagai and Vincent*, 2003].

[3] Water clarity, underwater light quality, the blueness of the water (spectral reflectance) and other optical properties of lakes are controlled by their inherent optical properties (IOPs), specifically absorption, *a*, and scattering, *b* (all acronyms and parameters are defined in the notation section). The IOPs depend only on the substances within the aquatic medium and not on the illumination conditions. By contrast, the apparent optical properties (AOPs) depend both on the medium and on the geometric structure of the ambient light field. The spectral absorption coefficient of natural waters, $a(\lambda)$ (m^{-1}), can be subdivided into four additive components:

$$a(\lambda) = a_w(\lambda) + a_{CDOM}(\lambda) + a_\phi(\lambda) + a_{NAP}(\lambda) \quad (1)$$

These components account for the contribution of water molecules (w), colored dissolved organic matter (CDOM), phytoplankton (ϕ) and nonalgal particles (NAP) to overall absorption at each wavelength, λ. Particle absorption, $a_p(\lambda)$, is represented by the sum of $a_\phi(\lambda)$ and $a_{NAP}(\lambda)$, where NAP is composed of heterotrophs such as bacteria, detritus, mineral particulates and bleached algal cells. Similarly, $b(\lambda)$ can be partitioned into the additive contributions from water molecules, b_w, and suspended

[1]Bigelow Laboratory for Ocean Sciences, West Boothbay Harbor, Maine, USA.
[2] Now at International Arctic Research Center, University of Alaska Fairbanks, Fairbanks, Alaska, USA.
[3]Département de Biologie et Centre d'Études Nordiques, Université Laval, Sainte-Foy, Québec, Canada.
[4]National Institute of Water and Atmospheric Research (NIWA), Christchurch, New Zealand.
[5]National Institute of Water and Atmospheric Research (NIWA), Hamilton, New Zealand.
[6]Lake Biwa Research Institute, Otsu, Japan.

0043-1397/04/2004WR003090

particles, b_p (dissolved substances are generally assumed to have a negligible contribution to scattering). In the field of hydrologic optics, case 1 waters are defined as those where all components except a_w and b_w are assumed to covary with chlorophyll *a* concentration (CHL*a*), and in these systems the IOPs can be estimated as a function of CHL*a* [*Morel*, 1988]. However, in coastal and inland ecosystems (case 2 waters), variations in the shape and magnitude of the $a(\lambda)$ and $b(\lambda)$ spectra are more complex, as are the relationships between CHL*a* and other components. *Babin et al.* [2003b] note that among the key questions that remain to be elucidated in this important class of waters is first whether robust relationships between $a_\phi(\lambda)$ and CHL*a* can be established, and secondly what determines $a_{NAP}(\lambda)$. The dependence of $b(\lambda)$ spectral shape and magnitude on particulate components also requires further attention [*Babin et al.*, 2003a], as does the particle backscattering coefficient, $b_{bp}(\lambda)$; i.e., the scattering occurring in the backward direction. This latter phenomenon strongly affects the spectral reflectance (and thus color) of lakes and oceans since backscattered photons are responsible for much of the upwelling light field in their surface waters. CDOM dynamics are also the object of active research in both marine and freshwater ecosystems. The relative importance of locally produced (autochthonous) CDOM versus that originating from soil and terrestrial vegetation decomposition in the catchment (allochthonous), and the variations in CDOM optical properties as a function of sources, composition and previous light exposure are topics of ongoing research and discussion.

[4] Lake Taupo, New Zealand, is the largest lake by volume in Australasia with an area of 620 km^2 and an average depth of 95 m. Like many large deep lakes throughout the world, Lake Taupo is oligotrophic and highly regarded for its blueness and transparency, and for its cultural, ecological and recreational values. At present approximately 10% of the catchment (total catchment area of 2673 km^2, excluding the lake) is tussock and exposed rock, 40% is native scrub and forest, 25% is exotic pine forest plantations and 25% is in pasture. The lake is located at latitude 38°S, experiences a maritime climate and is warm monomictic (annual overturn in winter). Maximum phytoplankton productivity in the lake occurs during the austral fall and winter when nutrients that have accumulated in the hypolimnion during stratification are mixed into the well-lit surface waters [*Vincent*, 1983]. Irradiance attenuation in the upper water column is generally lowest during late spring and summer when a lack of nutrients in the epilimnion limits phytoplankton growth. In the 1980s, nitrogen was shown to be the limiting nutrient [*Vincent*, 1983; *White et al.*, 1986], particularly during the stratified period when N:P ratios in Lake Taupo can drop to 4:1.

[5] In the present study, we undertook a detailed optical sampling program at Lake Taupo using state-of-the-art oceanographic instrumentation. This suite of measurements allowed us to quantify the effects of CDOM, and inorganic and organic particles in Lake Taupo on the absorption and scattering of solar irradiance in this system. The relationships established between optical properties and limnological variables provided insights into aspects of phytoplankton ecophysiology, particle composition, dissolved organic matter dynamics and the controls on lake water clarity and color.

2. Methods

2.1. Sampling

[6] Optical and biological measurements were made between 5 and 10 May 2002 at 19 stations distributed across Lake Taupo (Figure 1). The month of May (late fall) is a period of rapid phytoplankton growth leading toward the winter maximum in algal biomass and primary production in Lake Taupo [*Vincent*, 1983]. Water samples at all except the shallow inshore sites were collected at 10 m depth using a Niskin bottle and transferred immediately to dark polyethylene bottles. At riverine and shallow water stations at the south end of the lake (W15, W16, W17, and W18), surface water samples were collected. Samples were kept at ambient temperature (~15°C) until filtration (within 12 hours).

2.2. Ancillary Measurements

[7] Samples were filtered through GF/F filters for fluorometric determination of CHL*a* and pheopigments. Filters were frozen (−18°C) for up to 7 days before the pigments were extracted. Filters were then thawed and ground in 95% acetone before extracting overnight at 4°C. Fluorescence of centrifuged extracts was measured on a Turner F10-AU fluorometer (excitation 430 nm, emission 674 nm) before and after acidification. Total suspended solids (TSS) were measured gravimetrically, after filtering 1–1.5 L of water through preweighed, precombusted GF/F filter and drying to constant weight at 60°C. Nonvolatile suspended solids (NVSS) were determined by reweighing after combustion of these filters at 450°C for 3 h.

2.3. Inherent Optical Properties

[8] Vertical profiles of the absorption (*a*) and beam attenuation (*c*, the sum of $a + b$) coefficients at 9 wavelengths (412, 440, 488, 510, 532, 555, 650, 676, and 715 nm) were measured using an AC-9 absorption-attenuation meter (WETLabs Inc.). Profiles were made from the surface to 60–90 m (or to the bottom, at the shallower stations). Pure water calibration was performed on 4 of the 6 sampling days. Variability in pure water values was ±0.008 m^{-1} for *c* and ±0.010 m^{-1} for *a*, thus setting the instrument precision. The values of $a(715)$ were corrected for the temperature dependence of absorption according to the work of *Pegau et al.* [1997], and values of $a(\lambda)$ were corrected for the scattering error of the absorption tube by subtracting $a(715)$ from $a(\lambda)$ [see *Babin et al.*, 2003a]. Values for *a* and *b* (obtained by difference) were averaged over 1 m depth intervals from measurements taken every ~2 cm. The spectral shape of $b_p(\lambda)$ was obtained by a nonlinear fit at 9 discrete wavelengths measured using the AC-9 to the relationship:

$$b_p(\lambda) = b_p(555) \times (\lambda/555)^{-n} \quad (2)$$

where *n* is the hyperbolic exponent and the reference wavelength of 555 nm was chosen for comparison with previously published relationships [e.g., *Babin et al.*,

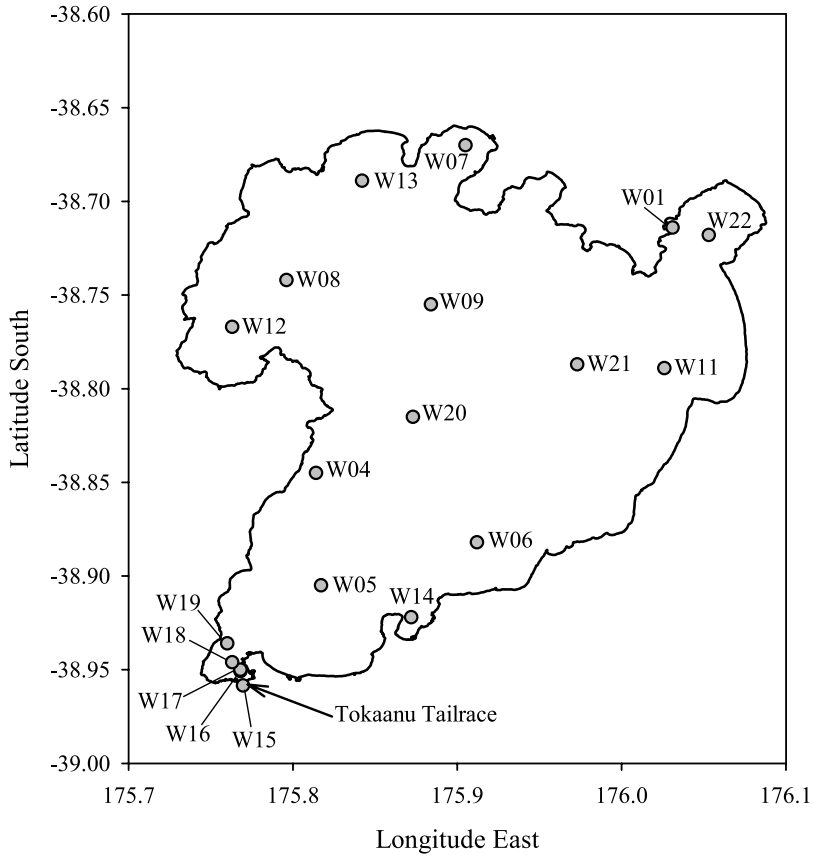

Figure 1. Map of the sampling stations in Lake Taupo.

2003a]. Similarly, the shape of the particulate attenuation spectrum, $c_p(\lambda)$, was obtained by nonlinear fitting to:

$$c_p(\lambda) = c_p(555) \times (\lambda/555)^{-\gamma} \quad (3)$$

where $c_p(\lambda)$ is equal to $c_{AC\text{-}9}(\lambda) - a_{CDOM}(\lambda)$ and γ is the hyperbolic exponent expressing the wavelength dependence following *Boss et al.* [2001]. On the basis of Mie particle optical theory, and supported by observations, *Twardowski et al.* [2001] demonstrated that the bulk particulate refractive index, $\overline{n}_p$, can be estimated from γ and the particle backscattering ratio (b_{bp}/b_p, the proportion of light scattered in the backward hemisphere by particles):

$$\overline{n}_p = 1 + b_{bp}/b_p^{0.5377+0.4867(\gamma)^2}\left[1.4676 + 2.2950(\gamma)^2 + 2.3113(\gamma)^4\right] \quad (4)$$

Although b_{bp}/b_p was not measured directly during this study, it was estimated from the results of Hydrolight simulations (see section 2.5).

[9] For particulate absorption measurement, samples (0.5 to 1 L) were vacuum filtered onto 25 mm Whatman GF/F filters that were stored at −18°C for <7 days. Particulate absorbance was measured over the spectral range 350–755 nm, at 2 nm resolution, using a Jasco 7850 spectrophotometer equipped with an integrating sphere (Jasco model TIS 417). Reference, baseline and path length amplification corrections were applied according to *Roesler* [1998]. Absorption by nonalgal particles, a_{NAP}, was estimated using the methanol extraction technique [*Kishino et al.*, 1985]. Because traces of residual pigment absorption were observed on most a_{NAP} spectra, the following equation was fitted to the $a_{NAP}(\lambda)$ spectra by nonlinear regression:

$$a_{NAP}(\lambda) = a_{NAP}(\lambda_o)\exp(-S_{NAP}(\lambda - \lambda_o)) \quad (5)$$

where λ_o is a reference wavelength and S_{NAP} is the parameter expressing the wavelength dependence. Following *Babin et al.* [2003b], the fit was performed over the spectral range 380–730 nm, excluding the 400–480 and 620–710 nm ranges to avoid the residual pigment absorption. The phytoplankton absorption coefficient was obtained by difference:

$$a_\phi(\lambda) = a_p(\lambda) - a_{NAP}(\lambda) \quad (6)$$

The inclusion of algal pigments within the chloroplasts, which in turn are contained within cells, causes a reduction in the absorption of pigmented particles relative to the absorption of the same pigments in solution [*Kirk*, 1994], and this so-called "package effect" has a major influence not only on light-harvesting capability of algal cells but also on the effect of algal cells on water column optical properties. The extent of the package effect was evaluated by dividing a_ϕ by CHL*a* to obtain the CHL*a*-specific phytoplankton absorption coefficient, a^*_ϕ.

[10] In the absence of direct measurements of CDOM, a_{CDOM} was determined by the difference between the AC-9

Table 1. Sampling Stations at Lake Taupo[a]

Site	Local Name	Date	Time	Depth, m	Mixed Layer, m	Euphotic Depth, m	Sky Condition
W01	Acacia Bay	5 May 2002	0930	42	42	26	clear sky
W04	Near Poukoura Pa	5 May 2002	1300	100	20	30	clear sky
W05	Kuratau Basin Site B	5 May 2002	1600	107	25	29	clear sky
W06	South of Motutaiko Is.	5 May 2002	1700	100	30	27	—
W07	Whangamata Bay	6 May 2002	1000	100	29	38	90% cloud
W08	Site C	6 May 2002	1130	115	31	39	80% cloud
W09	Lake centre	6 May 2002	1300	122	39	44	80% cloud
W11	Rotongaio Bay	6 May 2002	1500	112	42	n.a.	90% cloud
W12	Whanganui Bay	7 May 2002	1300	115	41	42	90% cloud
W13	Kawakawa Bay	7 May 2002	1430	113	39	35	20% cloud
W14	Motuopa Bay	8 May 2002	1500	25	6	21	—
W15	Tokaanu Tailrace	9 May 2002	1000	3	3	8	—
W16	0.7 km from Tailrace	9 May 2002	1025	4	1	16	—
W17	0.9 km from Tailrace	9 May 2002	1045	14	11	20	—
W18	1.3 km from Tailrace	9 May 2002	1135	38	37	24	—
W19	Mid Waihi Bay	9 May 2002	1400	75	50	25	clear sky
W20	Mid lake	10 May 2002	0930	100	39	35	90% cloud
W21	Site A	10 May 2002	1200	154	39	38	90% cloud
W22	Tapuaeharuru Bay	10 May 2002	1500	44	39	34	80% cloud

[a]Mixed layer depth was delimited by the depth where $\delta T > 0.2°C\ m^{-1}$. Euphotic depth (1% PAR) was determined from K_d(PAR) measured using a PUV500 radiometer. Sky condition is given only for stations where AOPs were measured.

measurement ($a_{AC\text{-}9}$, which includes particles and CDOM absorption but not absorption by water molecules) and the spectrophotometric measurement of particulate absorption at the nine wavelengths:

$$a_{CDOM}(\lambda) = a_{AC-9}(\lambda) - a_p(\lambda) \quad (7)$$

A nonlinear regression of these data was made using an exponential model of the form:

$$a_{CDOM}(\lambda) = a_{CDOM}(\lambda_o)\exp(-S_{CDOM}(\lambda - \lambda_o)) \quad (8)$$

This provided estimates of the magnitude of the absorption at reference wavelength λ_o, $a_{CDOM}(\lambda_o)$, and the parameter describing the wavelength dependence, S_{CDOM}. These fitted parameters and equation (8) were used to obtain full spectral values for $a_{CDOM}(\lambda)$.

2.4. Apparent Optical Properties

[11] Spectral diffuse attenuation coefficients for downward irradiance within the euphotic zone, $K_{dav}(\lambda)$ [*Kirk*, 1991], were calculated from irradiance measurements made using a HyperPro hyperspectral radiometer (Satlantic Inc). Irradiance profile measurements were done at 13 stations within 4 hours of local noon, during clear sky or relatively uniform overcast conditions (Table 1). Dark-corrected spectral downward irradiance, $E_d(\lambda, z)$, was measured every ~3 nm over the range 350–750 nm. Incident irradiance in air, $E_d(\lambda, 0^+)$, was measured simultaneously at 7 visible wavelengths using an OCR radiometer (Satlantic Inc) and these data were used to verify that the illumination was relatively constant during profiling (i.e., CV < 13% during one profile; part of the variability was often due to ship motion instead of variations in cloud cover). $K_{dav}(\lambda)$ was calculated from the slope of Ln $E_d(\lambda)$ vs. depth curve, where the maximum depth considered corresponded to the depth where irradiance at each λ was reduced to 1% of the value measured just under the surface. Separate estimates of K_{dav} for photosynthetically available radiation (PAR, 400–700 nm), K_{dav}(PAR), were also calculated from broadband E_d(PAR) measurements made using a PUV500 radiometer (Biospherical Instruments Inc.); as for $K_{dav}(\lambda)$, K_{dav}(PAR) was calculated from the slope of Ln E_d(PAR) vs. depth curve, where the maximum depth considered corresponded to the depth of 1% subsurface PAR.

[12] The HyperPro radiometer was also equipped with a downward looking sensor measuring spectral upwelling radiance (L_u). Because of its relevance to remote sensing applications, the ratio of L_u to E_d was measured at ~0.1 m depth using the HyperPro radiometer. $L_u(\lambda)/E_d(\lambda)$ generally showed little variability within the top ~1 m (apart from the increasing contribution of CHL*a* fluorescence with depth) and therefore no attempts were made to back extrapolate L_u/E_d to the exact 0^- depth (i.e., just under the water surface).

2.5. Forward Model for Spectral K_{dav} and L_u/E_d

[13] $K_d(\lambda)$ and $L_u(\lambda)/E_d(\lambda)$ were modeled from the IOPs and prevailing atmospheric conditions using the Hydrolight radiative transfer model [*Mobley*, 1994]. The Hydrolight model solves the radiative transfer equation from first principles using invariant imbedding methods to obtain the spectral radiance distribution as a function of depth, direction, and wavelength within and leaving the medium. Hydrolight first calculates the spectral radiance distribution, and then computes the AOPs $K_d(\lambda)$ and $L_u(\lambda)/E_d(\lambda)$. Hydrolight was run with the $a(\lambda)$ and $c(\lambda)$ profiles from the AC-9. Total absorption and attenuation were obtained by adding the pure water values to the AC-9 estimates (a_w from *Pope and Fry* [1997] and b_w from *Smith and Baker* [1981]). The CHL*a* fluorescence (with Hydrolight's default quantum efficiency of 0.02) and Raman scattering obtained from Hydrolight subroutines were included in the model.

[14] Atmospheric effects on the AOPs were accounted for in the Hydrolight simulations. The measured incident irradiance at 7 visible wavelengths was provided to Hydrolight for spectral interpolation. The built-in subroutine RADTRAN and HCNRAD determined the direct/diffuse ratio and angular distribution of this incident irradiance

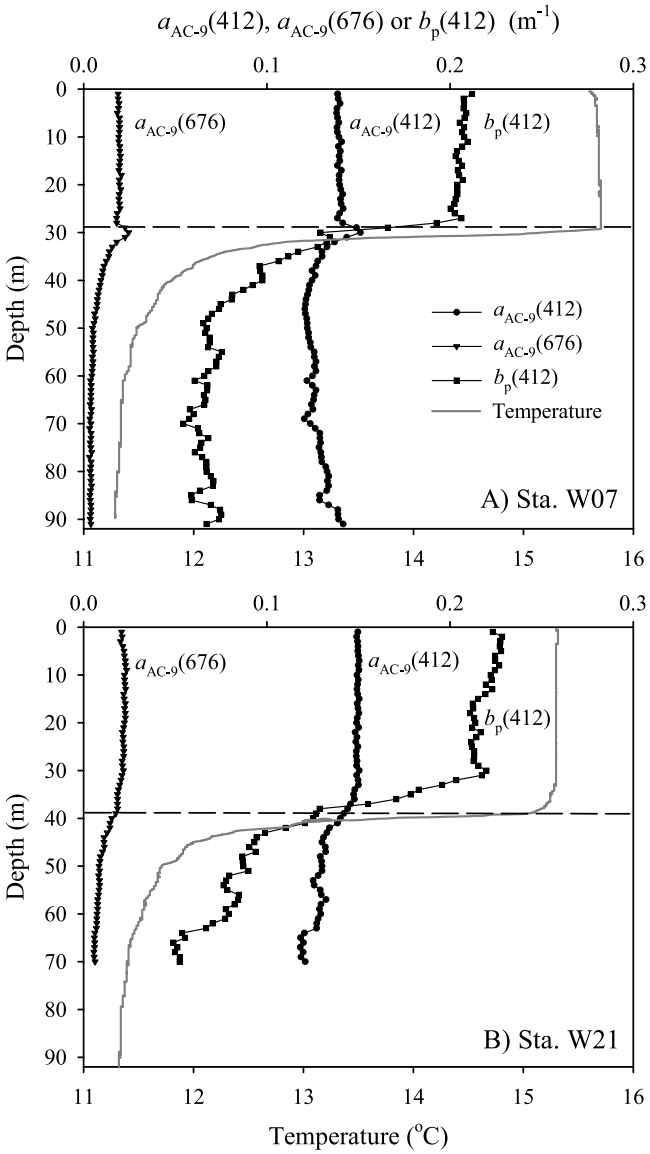

Figure 2. Vertical profiles of temperature, absorption coefficients at 412 nm and 676 nm, and scattering coefficient at 412 nm as measured using a WETLabs AC-9 at (a) Whangamata Bay (W07) and (b) at a center lake station (W21). Depth is 100 and 154 m at stations W07 and W21, respectively, and the mixed layer depth was 29 and 39 m at stations W07 and W21, respectively (as shown by a dashed line).

based on GMT time, location, percent cloud cover and atmospheric parameters. Default atmospheric parameters were: Air mass type = 5, relative humidity = 80%, precipitable water = 2.5 cm, visibility = 15 km, wind speed = 2.5 m s^{-1} and total ozone was calculated from the built-in climatology. When RADTRAN was used to determine incident $E_d(\lambda)$ instead of supplying the measured values, this set of atmospheric parameters gave a good fit (within 15%) to incident E_d measured during clear sky conditions. For overcast conditions, the percent cloud cover in the model was adjusted so that modeled incident $E_d(\lambda)$ was within 15% of measured values.

[15] Using Hydrolight, it was possible to check the consistency of the input IOPs and atmospheric parameters by comparing the modeled $K_d(\lambda)$ and $L_u(\lambda)/E_d(\lambda)$ to those measured using the HyperPro radiometer. The measured $K_{dav}(\lambda)$ was compared to the measured $K_d(\lambda)$ prevailing just under the surface. Although K_d varied with depth as a result of the modification of the angular irradiance distribution, the maximum difference within the depth interval from the surface to the 1% depth was less than ~8% across all wavelengths. Because L_u/E_d is much more sensitive than K_d to the particle backscattering ratio b_{bp}/b_p [*Gordon*, 1993] the comparison of measured and modeled L_u/E_d allowed us to estimate b_{bp}/b_p and hence the appropriate phase function (function describing the angular distribution of the scattered photons with units of sr^{-1}). For each station, the "best" Fournier-Forand phase function (assuming that the b_{bp}/b_p ratio is wavelength independent; Hydrolight uses the Fournier-Forand analytic functions to describe the phase function) was determined by varying the b_{bp}/b_p ratio until the best fit of the modeled to measured $L_u(\lambda)/E_d(\lambda)$ was obtained. Note that the b_{bp}/b_p ratio was the only IOP that was optimized in our simulations.

3. Results

3.1. Spatial and Vertical Variations of the IOPs in Lake Taupo

[16] In early May, during the period of early winter mixing and deep water entrainment, the IOPs were remarkably homogenous in the mixed layer of Lake Taupo throughout its 620 km^2 basin. For example, with the exception of station W15, which was located in flowing water at the mouth of the Tokaanu Tailrace (the larger inlet of Lake Taupo), $a_{AC-9}(412)$ varied over the narrow range 0.14–0.22 m^{-1}, and $b_p(412)$ varied over the range 0.21–0.41 m^{-1}. The IOPs also exhibited relatively little vertical variability in the well-mixed upper ~30 m (Figure 2). Scattering was about 2–4 times higher in the epilimnion compared to the hypolimnion and $a_{AC-9}(676)$, indicative of CHL*a* absorption, was about 4–5 times higher in the epilimnion than in the hypolimnion (Figure 2).

3.2. Absorption Coefficient and Its Relation to Optically Active Substances

[17] Particle absorption showed little variability in magnitude and shape across the lake (Figure 3a) despite sampling stations located up to 45 km apart and differing widely in water depth (from 4 m near the Tokaanu Tailrace to 154 m near the deepest part of the lake; Table 1). This relatively narrow range of a_p is in agreement with the small variations observed in suspended particle mass (0.35–0.85 mg L^{-1}, Table 2) and CHL*a* (0.86–1.21 μg L^{-1}, Table 2). However, at the river station W15 a_p was about 3 times higher (Figure 4), and material of river origin was likely responsible for the slightly higher values measured at the nearby stations W16 and W17 (Figure 3a).

[18] As indicated by the presence in the a_p spectra of peaks typical of phytoplankton pigments absorption, phytoplankton was responsible for a large part of a_p (Figure 3b); for example at 443 nm, near the position of the red absorption peak of CHL*a*, a_ϕ represented 53–82% of a_p. The spectral shape of $a_\phi(\lambda)$ indicated a significant contribu-

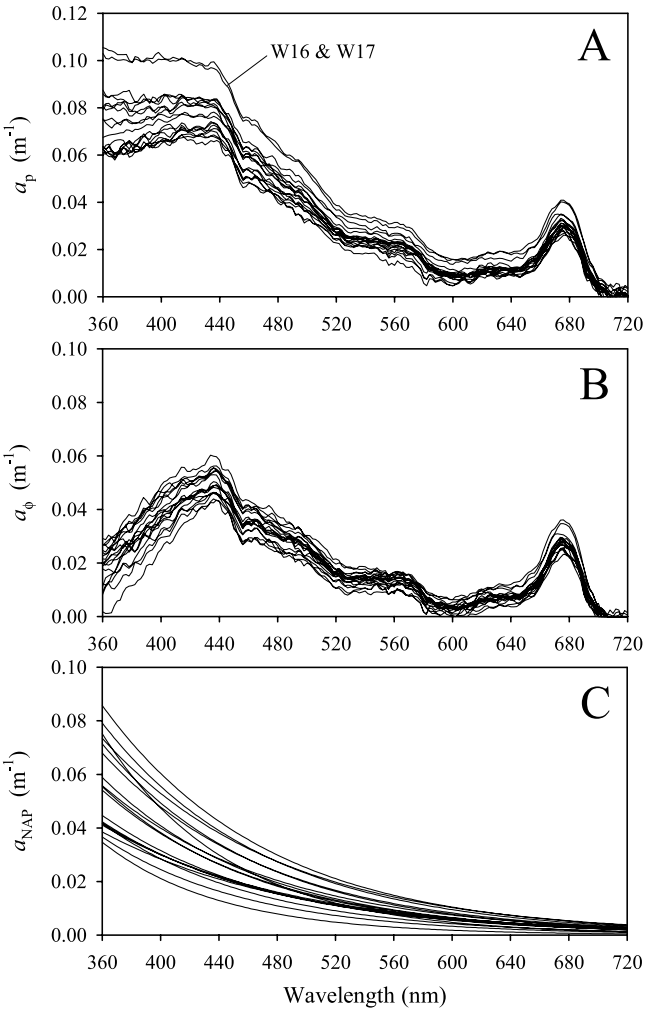

Figure 3. Particle absorption spectra at 10 m depth for the 18 stations sampled in Lake Taupo (values for the river station W15 are illustrated at Figure 4). (a) Total particle absorption, a_p, (b) phytoplankton absorption, a_ϕ, and (c) nonalgal particles absorption a_{NAP}. For the three shallow stations located near the Tokaanu Tailrace, surface values are presented. Measured a_{NAP} was fitted to equation (5), excluding the 400–480 and 620–710 nm ranges to avoid the residual pigment absorption, and fitted spectra are presented in Figure 3c.

tion by cyanobacteria and chlorophytes with shoulders at 520–580 nm consistent with phycoerythrin (cyanobacteria [*Kirk*, 1994]), and at 620–650 nm indicative of chlorophyll *b* (chlorophytes [*Kirk*, 1994]). Microscopic examination of samples collected one week after the optical survey revealed dominance by a mixture of phytoplankton groups, including species of *Asterionella*, *Ceratium*, *Anabaena*, *Dinobryon* and *Botryococcus*. The CHL*a*-specific phytoplankton absorption coefficient at 674 nm, $a^*_\phi(674)$, varied between 0.020–0.033 m^{-1} (μg L)$^{-1}$ (mean = 0.027 m^{-1} (μg L)$^{-1}$). This high $a^*_\phi(674)$ value suggests minimal package effect consistent with small cells, high light acclimation or nutrient limitation [*Bricaud et al.*, 1995; *Stramski et al.*, 2002]. Pheopigments (PHEO) represented on average 15% of the sum of CHL*a* and PHEO; including the PHEO concentration within the CHL*a* estimate (as in the work by *Bricaud et al.* [1995]) would lower the average $a^*_\phi(674)$ to 0.023 m^{-1} (μg L)$^{-1}$, which remains within the range of minimal package effect.

[19] The nonalgal particles absorption, a_{NAP}, was slightly more variable than a_ϕ (Figure 3c). S_{NAP} varied from 0.008 to 0.012 nm^{-1}, (mean = 0.009 nm^{-1}), falling at the low range of published values [*Roesler et al.*, 1989; *Babin et al.*, 2003b]. The average $a_{NAP}(443)$:TSS ratio was 0.05 m^2 g^{-1} with a 34% coefficient of variation (CV). This value is close to that found by *Babin et al.* [2003b] in coastal waters around Europe, i.e., 0.04 m^2 g^{-1}, CV = 56%. Note however that this ratio is slightly more variable than a_{NAP} itself (CV = 29% at 443 nm) or the ratio a_{NAP}:CHL*a* (CV of 28% at 443 nm). At the river station W15, the $a_{NAP}(443)$:TSS ratio was 0.13 m^2 g^{-1}, a value more typical of mineral particles with a high content of iron, a major pigmenting agent [*Babin and Stramski*, 2004].

[20] CDOM absorption at 443 nm varied 0.03–0.09 m^{-1} (Figure 5), with the highest values found at the shallow stations near the Tokaanu Tailrace (W16, W17, W18, and W19) and at station W14 in Motuopa Bay. CDOM absorption at the river station W15 was high ($a_{CDOM}(443)$ = 0.41 m^{-1}; Figure 4) and the slightly higher values near the Tokaanu Tailrace likely reflected the input from the river. S_{CDOM} varied over the range 0.013–0.024 nm^{-1} (mean = 0.017 nm^{-1}). S_{CDOM} was correlated to $a_{CDOM}(443)$, decreasing as $a_{CDOM}(443)$ increased (r = −0.780, P = <0.001, N = 18). S_{CDOM} at the river station was 0.014 nm^{-1}, in agreement with this trend. There was no significant correlation between $a_{CDOM}(443)$ and CHL*a* concentrations (P = 0.669, N = 18).

[21] Figure 6 illustrates the absorption budget derived from our data as ternary diagrams [*Sathyendranath*, 2000] at three different wavelengths. The diagrams underscore

Table 2. Chlorophyll *a* Concentration (CHL*a*), Total Suspended Solids (TSS), Percent of TSS Represented by Nonvolatile Suspended Solids (NVSS%), and Relevant IOPs[a]

Site	CHL*a*, μg L^{-1}	TSS, mg L^{-1}	NVSS%	b_{bp}/b_p	n	γ	$\overline{n}_p$
W01	1.06	0.55	15	0.011	0.41	0.88	1.08
W04	0.86	0.40	<5	0.011	0.76	1.14	1.04
W05	0.87	0.40	<5	0.008	0.71	1.07	1.04
W06	1.13	0.60	15	n.a.	0.63	0.99	n.a.
W07	1.02	0.50	<5	0.013	0.63	1.09	1.06
W08	1.11	0.55	<5	0.010	0.79	1.21	1.03
W09	1.08	0.40	<5	0.010	0.78	1.21	1.03
W11	1.10	0.50	15	0.011	0.62	0.96	1.07
W12	1.11	0.45	<5	0.012	0.69	1.13	1.05
W13	1.06	0.50	<5	0.014	0.70	1.10	1.06
W14	1.07	0.60	30	n.a.	0.59	0.95	n.a.
W15	2.59	1.60	55	n.a.	0.64	1.08	n.a.
W16	1.21	0.70	25	n.a.	0.41	0.72	n.a.
W17	1.60	0.55	20	n.a.	0.53	0.93	n.a.
W18	0.82	0.85	5	n.a.	0.55	0.86	n.a.
W19	0.96	0.70	10	0.012	0.57	0.97	1.07
W20	0.86	0.35	<5	0.013	0.72	1.09	1.06
W21	1.03	0.40	<5	0.011	0.72	1.16	1.04
W22	1.09	0.60	20	0.013	0.61	1.01	1.07

[a]The b_{bp}/b_p value gives the best fit to measured L_u/E_d, n is an exponent expressing the wavelength dependence of $b_p(\lambda)$, γ is an exponent expressing the wavelength dependence of $c_p(\lambda)$, and $\overline{n}_p$ is estimated bulk refractive index calculated according to equation (4); n.a. is not available.

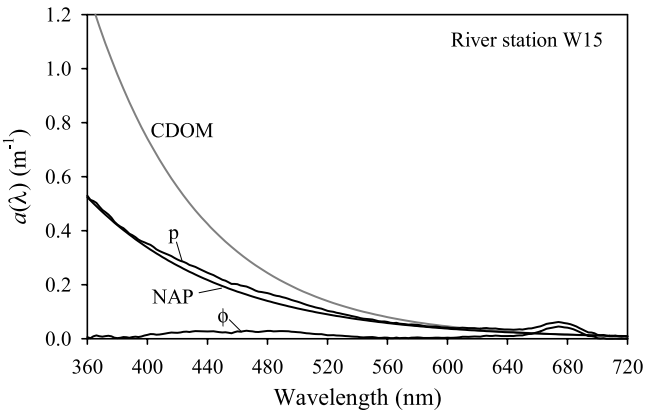

Figure 4. Absorption spectra of CDOM (a_{CDOM}), total particles (a_p), phytoplankton (a_ϕ) and nonalgal particles (a_{NAP}) at the river station W15.

the low variability in contribution of each component to the total absorption in Lake Taupo in early May, and the proportionally much lower contribution of a_ϕ in the river waters. CDOM was dominant at UV wavelengths (Figure 6a) and phytoplankton dominated in the red region (Figure 6c). Figure 6b shows that the "blueness" of Lake Taupo is equally affected by phytoplankton, NAP and CDOM, and therefore all three components must be taken into account in order to understand and predict the water color of this lake.

3.3. Scattering Coefficient and Its Relation to Optically Active Substances

[22] The particle scattering coefficient at 555 nm, $b_p(555)$, varied 0.18–0.37 m^{-1}, and was strongly correlated to TSS concentration (Figure 7a). The average mass-specific $b_p(555)$ was 0.44 $m^2\ g^{-1}$ (CV = 17%); at station W15 it was 0.54 $m^2\ g^{-1}$. These values are in agreement with the value of 0.5 $m^2\ g^{-1}$ found in case 2 marine waters by *Babin et al.* [2003a]. There was no significant correlation between $b_p(555)$ and CHL*a* (P < 0.123, N = 18). The spectral shape of $b_p(\lambda)$ (Figure 7b) was well defined by the hyperbolic shape of equation (2), although

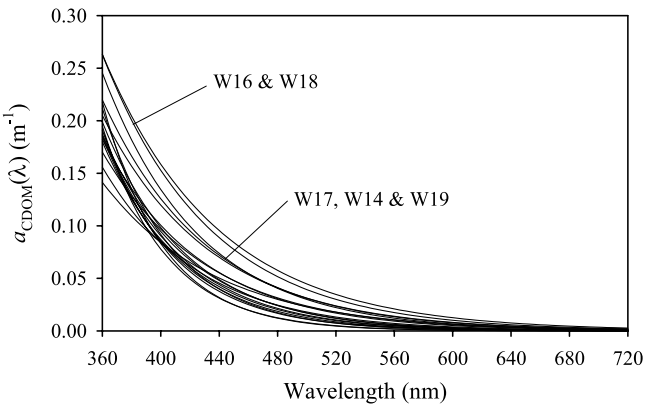

Figure 5. Absorption spectra of CDOM (a_{CDOM}) for the 18 stations sampled in Lake Taupo. In absence of direct measurement, a_{CDOM} was estimated as the difference between $a_{AC\text{-}9}$ and a_p fitted to the exponential model of equation (8) (see section 2.3).

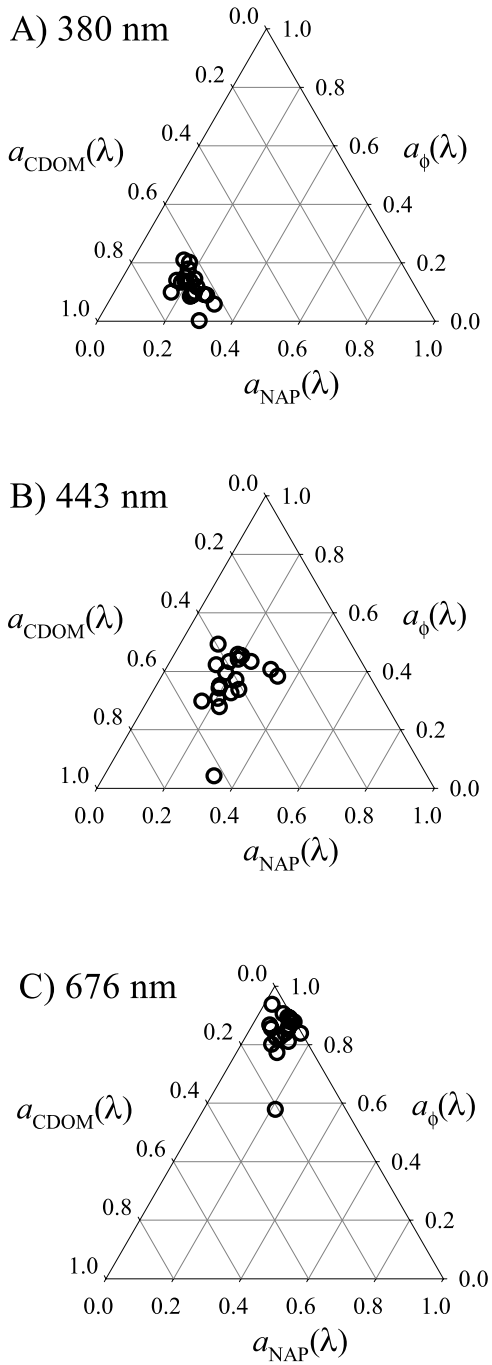

Figure 6. Ternary diagrams of the absorption budget for the 19 stations in Lake Taupo at (a) 380 nm, (b) 443 nm, and (c) 676 nm. The data point markedly different from the others corresponds to the river station W15. The three wavelengths were chosen to allow comparison with Figure 16 of *Babin et al.* [2003b]; 380 nm is a representative UV-A wavelength, 443 nm is in the blue region of the spectrum near the main absorption peak of phytoplankton, and 676 nm corresponds to the red absorption peak of CHL*a*.

deviations from the hyperbolic shape were evident at the position of absorption peaks (a phenomenon consistent with particle optical theory [see *Babin et al.*, 2003a]). The average value for *n*, the hyperbolic exponent of the $b_p(\lambda)$ spectra, was 0.63 (range 0.41–0.79, Table 2). The *n*

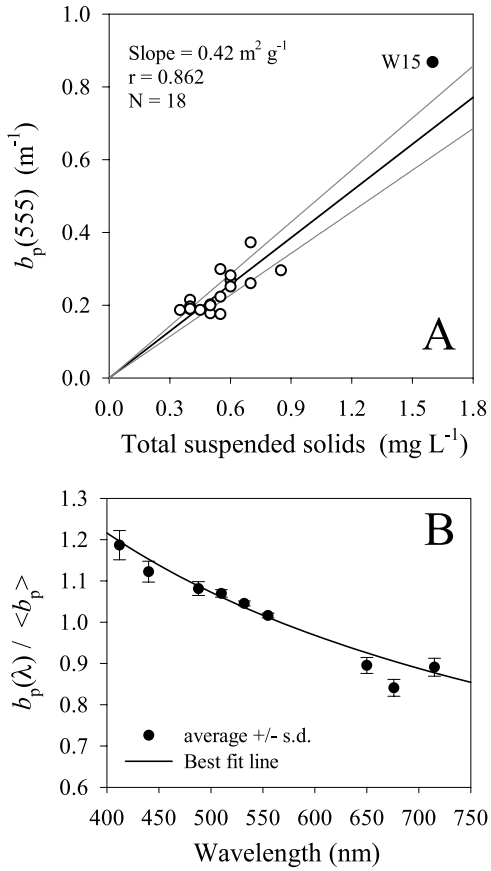

Figure 7. (a) Correlation between the particle scattering coefficient at 555 nm, $b_p(555)$, and total suspended solids (TSS); (b) spectral variation in b_p illustrated by the average spectra (±1 standard deviation) of the $b_p(\lambda)/\langle b_p \rangle$ ratio, where $\langle b_p \rangle$ is the spectrally averaged scattering coefficient of particles. The river station W15 was excluded from the regression in Figure 7a and was not included in the average spectra presented in Figure 7b.

exponent was strongly correlated to γ, the hyperbolic exponent of the $c_p(\lambda)$ spectra ($n = 0.786\ \gamma - 0.172$; r = 0.930) (Table 2) which is expected given that both n and γ are affected by the particles size distribution and their index of refraction [*Boss et al.*, 2001; *Twardowski et al.*, 2001; *Babin et al.*, 2003a].

[23] The comparison of modeled and measured L_u/E_d allowed the backscattering ratio b_{bp}/b_p to be estimated. The best fit between modeled and measured L_u/E_d was obtained using the b_{bp}/b_p ratio of the Fournier-Forand phase function that varied 0.008–0.014 (Table 2) with a mean value of 0.011 (note that b_{bp}/b_p is available only for stations where L_u/E_d was measured). From b_{bp}/b_p and γ, we calculated that the bulk particulate refractive index, $\overline{n}_p$, varied 1.03–1.08 in the surface waters of Lake Taupo (Table 2), which indicates a preponderance of organic particles [*Twardowski et al.*, 2001; *Babin et al.*, 2003a].

3.4. Measured Apparent Optical Properties

[24] The spectral shape and magnitude of K_{dav} showed very little variability between the 13 sampled stations (Figure 8a). At all stations, $K_{dav}(\lambda)$ was characterized by high attenuation in the red part of the spectrum and comparatively low attenuation in the green-blue, as expected in an oligotrophic lake with relatively low a_{CDOM} and low phytoplankton biomass. The minimum K_{dav} was at ~495–500 nm (Figure 8a, inset). The variability in magnitude of L_u/E_d measured at the 13 stations (Figure 8b) was approximately the same as observed for K_{dav} (e.g., at 500 nm, the CV was 13% and 14% for L_u/E_d and K_{dav}, respectively). Maximum L_u/E_d was in the blue-green region of the spectrum at ~480–495 nm, and it varied 0.004–0.006 sr^{-1}. Mostly because of absorption by water molecules, L_u/E_d was low in the red part of the spectrum.

3.5. Modeling of Downwelling Irradiance Attenuation and Reflectance From the IOPs

[25] There was a good agreement between $K_d(\lambda)$ modeled from the IOPs using Hydrolight and $K_{dav}(\lambda)$ measured using the HyperPro radiometer (three stations representing extremes in K_d, CHL*a* concentration and atmospheric conditions are illustrated in Figures 9a, 9b, and 9c). The measured L_u/E_d ratios were also well reproduced by the model (Figures 9d, 9e, and 9f). Typically, the difference

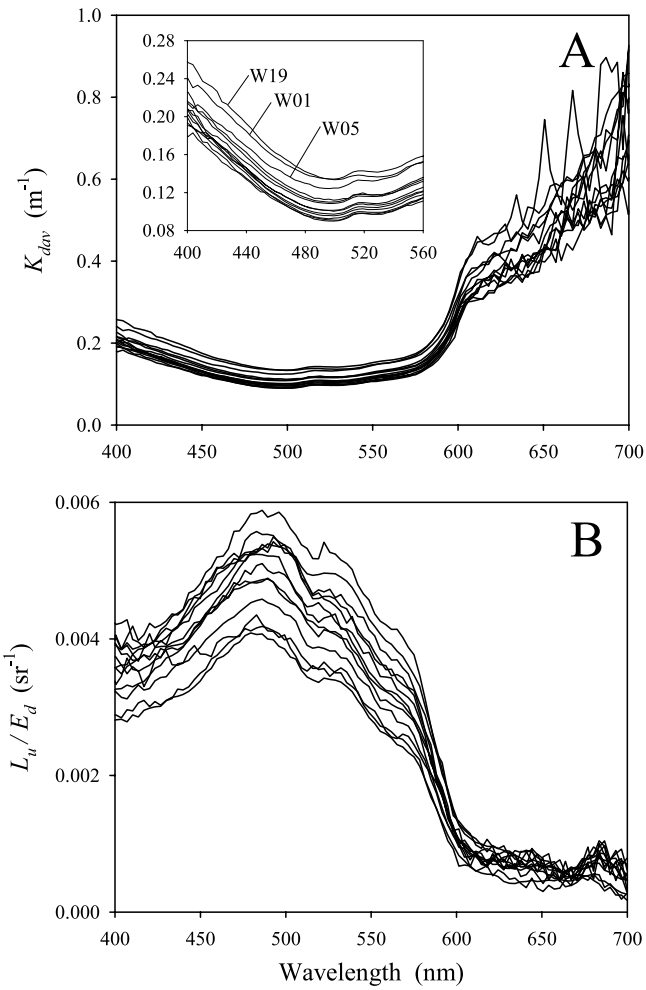

Figure 8. Apparent optical properties measured using an HyperPro radiometer. (a) Spectral attenuation coefficients for downwelling irradiance within the euphotic zone, K_{dav}; (b) ratio of upwelling radiance to downwelling irradiance measured at ~0.1 m depth, L_u/E_d. The inset in Figure 8a shows detailed K_{dav}(400–560).

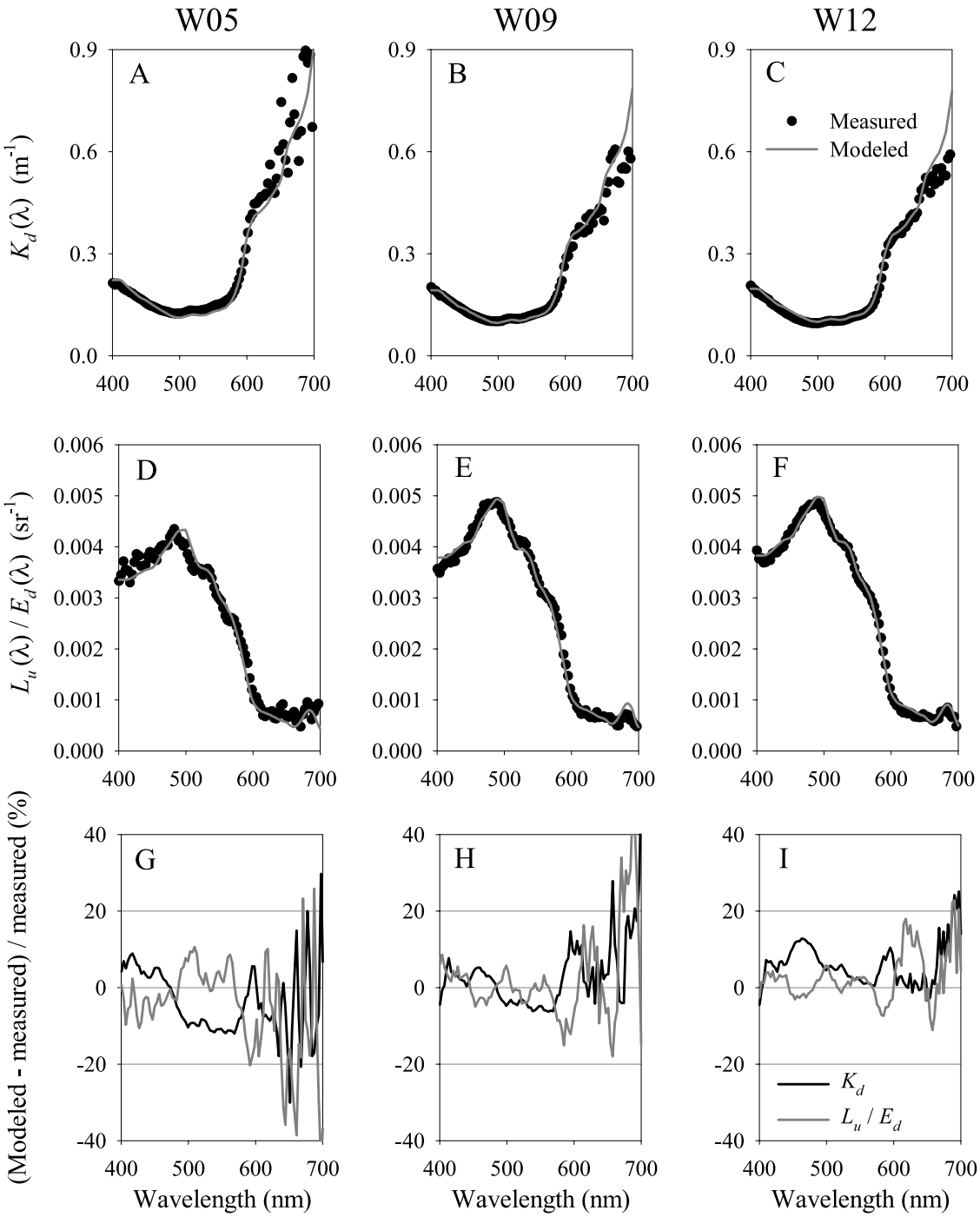

Figure 9. Measured and modeled $K_d(\lambda)$ and $L_u(\lambda)/E_d(\lambda)$ and the percent difference between modeled and measured values at three stations representing extremes in K_d, CHL*a* concentration, and atmospheric conditions. (a, d, and g) Station W05 at 16h00, clear sky, $b_{bp}/b_p = 0.008$. (b, e, and h) Station W09 at 13h00, overcast $b_{bp}/b_p = 0.010$. (c, f, and i) Station W12 at 13h00, overcast, $b_{bp}/b_p = 0.012$. See color version of this figure at back of this issue.

between modeled and measured $K_d(\lambda)$ or $L_u(\lambda)/E_d(\lambda)$ was <15%, except in the red part of the spectrum where the difference was up to 40% (Figures 9g, 9h, and 9i). The shape of the difference spectrum suggests a random error; there is no suggestion of any systematic deviation over most of the PAR wave band (note that part of the difference in peaks position results from the limited spectral resolution of the *a* and *c* profiles used as input to the model). Because L_u/E_d is much more sensitive than K_d to the particle backscattering ratio (b_{bp}/b_p), comparison of measured and modeled L_u/E_d allowed a much better estimation of b_{bp}/b_p (Table 2) than would be possible from comparison of K_d spectra. For example, at station W09 near the center of the lake (Figure 9e), doubling b_{bp}/b_p from 0.01 to 0.02 increases $K_d(\lambda)$ by at most 5% (at λ = 550 nm) while it increases $L_u(\lambda)/E_d(\lambda)$ by up to 67% (at λ = 700 nm).

[26] Hydrolight allowed the impact of factors other than the IOPs to be evaluated. For the conditions prevailing in

Lake Taupo at the time of this study, the inclusion of Raman scattering and CHL*a*-fluorescence decreased K_d by less than 1%. Inclusion of CDOM fluorescence as parameterized in the Hydrolight subroutine would also decrease K_d by less than 1%. Differences in time of the day and sky conditions had a higher impact on K_d. For example, for the IOPs prevailing at station W09, the difference between measurements made at 12h00 and measurements made at 16h00 would be 8–14% (depending on wavelength). Similarly, a 90% cloud cover would decrease K_d by 3–4% relative to measurements made at noon on a clear day. L_u/E_d was less sensitive to sky conditions with differences in time of the day or cloud cover causing <2% variations.

4. Discussion

4.1. Optical Properties of Lake Taupo

[27] Our detailed observations of the optical regime of Lake Taupo over 6 days during the season of maximum phytoplankton net growth rates showed relatively homogenous conditions throughout this large lake, and the equal roles of CDOM, phytoplankton and nonalgal particles in controlling water transparency and color at blue wavelengths (Figure 6b). Our study takes advantage of recent advances in methodology and instrumentation, thereby improving previous attempts to link the optically active substances present in lakes to the IOPs and AOPs [e.g., *Howard-Williams and Vincent*, 1984; *Vertucci and Likens*, 1989, and references therein; *Gallegos et al.*, 1990]. Interestingly, the relationships we established between the IOPs and the optically active substances in Lake Taupo are consistent with relationships previously found in marine waters [e.g., *Babin et al.*, 2003a, 2003b; *Roesler et al.*, 1989], suggesting a uniformity within particle optical properties that crosses the fresh/marine water boundaries.

[28] Useful information regarding the nature of suspended particles can be inferred from the IOPs. For example, the relatively low values of the a_{NAP}:TSS ratio and low $\overline{n}_p$ in the surface waters of Lake Taupo indicate a preponderance of organic particles over mineral particles consistent with the observed low proportion of NVSS relative to TSS (Table 2). The strong correlation between $b_p(555)$ and TSS and the absence of significant correlation between $b_p(555)$ and CHL*a* suggested that scattering particles in Lake Taupo varied independently from phytoplankton biomass. The IOPs also contain valuable information that is relevant to phytoplankton ecophysiology. The high $a_\phi(674)$* indicated minimal package effect consistent with small cells, high light acclimation or nitrogen limitation [e.g., *Stramski et al.*, 2002; *Babin et al.*, 2003b]. At the time of the study, the mixed layer depth rarely exceeded the depth of the euphotic zone (Table 1) suggesting that the cells were likely to be adapted to relatively high light. The shape of $a_\phi(\lambda)$ indicated a significant contribution by cyanobacteria and chlorophytes to total phytoplankton absorption. The observed a_ϕ spectra and the dominant phytoplankton groups revealed by microscopy are consistent with our understanding of the seasonal species succession in this lake [*Vincent and Forsyth*, 1983]. Picocyanobacteria were not enumerated in the present study, but they are also likely to have been important contributors to the overall phytoplankton biomass, as in low DOC, oligotrophic lakes elsewhere [*Vincent*, 2000; *Drakare et al.*, 2003].

[29] During this survey of Lake Taupo optics, there was no correlation between a_{CDOM} and CHL*a*. The Tokaanu Tailrace appeared to be a significant source of CDOM to the lake, with the higher S_{CDOM} associated with low a_{CDOM} values measured away from the river, consistent with an increase of S_{CDOM} in the visible wave band during the photochemical degradation of CDOM [*Twardowski and Donaghay*, 2002]. Although longer-term studies would be needed in order to determine the relative importance of allochthonous vs. autochthonous CDOM, these results would suggest that a_{CDOM} in Lake Taupo is essentially a function of the balance between allochthonous inputs and photochemical degradation. The observations imply that the CDOM is largely independent of autochthonous phytoplankton production and decoupled in time or space from phytoplankton biomass/production.

4.2. From the IOPs to K_{dav} and L_u/E_d

[30] The Hydrolight model proved to be a powerful tool for translating the measured IOPs into AOPs (K_d and L_u/E_d). Hydrolight offers advantages over less sophisticated models based on Monte Carlo simulations [e.g., *Kirk*, 1991; *Morel and Loisel*, 1998; *Belzile et al.*, 2002]; for example it allows a better representation of the atmospheric conditions and their impact on the incident irradiance, and it also allows the inclusion of vertical variability. Hydrolight simulations showed that the observed variability in K_{dav} and L_u/E_d was in part due to differences in solar zenith angle and sky conditions prevailing at the time of measurement rather than variation in IOPs. Hydrolight generally predicted the measured AOPs within 15% (Figure 9; some deviations up to 40%), indicating that the IOPs inputs to the model were accurate. Our capability to reproduce the measured K_d and L_u/E_d from the measured IOPs and atmospheric conditions provide the basis for the development of models that could simulate the impact of changes in optically active substances.

[31] One valuable outcome of our modeling effort is the estimation of the particle backscattering ratio, b_{bp}/b_p. This IOP is rarely measured in lakes although crucial for remote sensing applications as well as for estimating particle composition [*Twardowski et al.*, 2001]. It is of interest that the often used San Diego Harbor particle phase function measured by *Petzold* [1972] has a $b_{bp}/b_p = 0.018$ [*Mobley*, 1994], a value that is much too high to reproduce the L_u/E_d spectra of Lake Taupo. *Mobley et al.* [2002] also found the San Diego Harbor phase function to have a b_{bp}/b_p higher than that of the case 2 water off the coast of New Jersey. Together, these results suggest that, even in case 2 waters, the San Diego Harbor phase function is inappropriate and that other phase functions having a lower b_{bp}/b_p might be more representative. Use of a spectrally independent b_{bp}/b_p within the Fournier-Forand phase function of Hydrolight yielded a good fit between modeled and measured $L_u(\lambda)/E_d(\lambda)$, suggesting that the spectral dependence of b_{bp}/b_p is negligible for these waters. This is in agreement with the weak (<10%) spectral dependence of b_{bp}/b_p found by *Twardowski et al.* [2001] in case 1 and case 2 waters of the Gulf of California. The implications that the $b_{bp}(\lambda)$ has nearly the same spectral dependence as $b_p(\lambda)$ has proven to be useful in determining bulk particle

composition [e.g., *Twardowski et al.*, 2001] and for constraining the inversion of water color [e.g., *Roesler and Boss*, 2003].

5. Conclusions

[32] Like many oligotrophic lakes elsewhere, the need to protect Lake Taupo's renowned water clarity has been identified as the key public issue facing this highly valued natural resource, with implications for community values including cultural issues, water appearance, drinking water, recreational usage and tourism [*James et al.*, 2003]. The relationships we established between the IOPs and the optically active substances in Lake Taupo provide insights into the controls on optical properties of freshwater ecosystems where water quality as indicated by transparency and color is of interest and concern for water resources management. This level of understanding is needed for future remote sensing of water quality parameters, and for predicting the impacts of natural and human-induced environmental change on freshwater ecosystems.

Notation

a_x absorption coefficient, where x = w, CDOM, ϕ, NAP, p and AC-9 specifies water, dissolved organic matter, phytoplankton, nonalgal particles, total particles, and the sum of dissolved and particulate, respectively, m^{-1}.

a^*_ϕ phytoplankton chlorophyll *a*-specific absorption coefficient, m^{-1} (μg L)$^{-1}$.

b_x scattering coefficient, where x = w, ϕ, NAP, and p specifies water, phytoplankton, nonalgal particles, and total particles, respectively, m^{-1}.

b_{bp} particle backscattering coefficient, m^{-1}.

b_{bp}/b_p particle backscattering ratio, dimensionless.

c_x beam attenuation coefficient, where x = p and AC-9 specifies particles and the sum of dissolved and particulate, respectively, m^{-1}.

$E_d(z)$ downward irradiance at depth z, W m^{-2} nm^{-1}.

γ exponent of the hyperbolic fit to the $c_p(\lambda)$ spectrum (equation (3)), dimensionless.

K_d vertical attenuation coefficient for downward irradiance, m^{-1}.

K_{dav} K_d determined over the depth interval from the surface to the depth of 1% subsurface irradiance at each λ, m^{-1}.

L_u upwelling radiance, W m^{-2} $sr^{-1}nm^{-1}$.

n exponent of the hyperbolic fit to the $b(\lambda)$ spectrum (equation (2)), dimensionless.

$\overline{n}_p$ bulk particulate refractive index, dimensionless.

S_{CDOM} parameter expressing the wavelength dependence of the CDOM absorption spectrum (equation (8)), nm^{-1}.

S_{NAP} parameter expressing the wavelength dependence of the nonalgal particle absorption spectrum (equation (5)), nm^{-1}.

[33] **Acknowledgments.** We thank Richard Staines, Max Gibbs and Bob Spigel for assistance in the field and the New Zealand Foundation for Science and Technology, Japan Science and Technology Agency, Natural Sciences and Engineering Research Council of Canada, Tuwharetoa Māori Trust Board, the Canada Research Chair program, and the Fonds Québécois de la Recherche sur la Nature et les Technologies for funding support. We also thank Emmanuel Boss and an anonymous reviewer for insightful comments. This is a contribution to TAUPEX 2002 sponsored by the National Institute of Water and Atmospheric Research (NIWA) New Zealand.

References

Babin, M., and D. Stramski (2004), Variations in the mass-specific absorption coefficient of mineral particles suspended in water, *Limnol. Oceanogr.*, *49*, 756–767.

Babin, M., A. Morel, V. Fournier-Sicre, F. Fell, and D. Stramski (2003a), Light scattering properties of marine particles in coastal and open ocean waters as related to the particle mass concentration, *Limnol. Oceanogr.*, *48*, 843–859.

Babin, M., D. Stramski, G. M. Ferrari, H. Claustre, A. Bricaud, G. Obolensky, and N. Hoepffner (2003b), Variations in the light absorption coefficients of phytoplankton, non-algal particles, and dissolved organic matter in coastal waters around Europe, *J. Geophys. Res.*, *108*(C7), 3211, doi:10.1029/2001JC000882.

Belzile, C., W. F. Vincent, and M. Kumagai (2002), Contribution of absorption and scattering to the attenuation of UV and photosynthetically available radiation in Lake Biwa, *Limnol. Oceanogr.*, *47*, 95–107.

Boss, E., M. S. Twardowski, and S. Herring (2001), Shape of the particulate beam attenuation spectrum and its inversion to obtain the shape of the particulate size distribution, *Appl. Opt.*, *40*, 4885–4892.

Bricaud, A., M. Babin, A. Morel, and H. Claustre (1995), Variability in the chlorophyll-specific absorption coefficients of natural phytoplankton: Analysis and parameterization, *J. Geophys. Res.*, *100*, 13,321–13,332.

Drakare, S., P. Blomqvist, A.-K. Bergström, and M. Jansson (2003), Relationships between picophytoplankton and environmental variables in lakes along a gradient of water colour and nutrient content, *Freshwater Biol.*, *48*, 729–740.

Gallegos, C. L., D. L. Correll, and J. W. Pierce (1990), Modeling spectral diffuse attenuation, absorption, and scattering coefficients in a turbid estuary, *Limnol. Oceanogr.*, *35*, 1486–1502.

Goldman, C. R. (1988), Primary productivity, nutrients, and transparency during the early onset of eutrophication in ultra-oligotrophic Lake Tahoe, California-Nevada, *Limnol. Oceanogr.*, *33*, 1321–1333.

Gordon, H. R. (1993), The sensitivity of radiative transfer to small-angle scattering in the ocean: A quantitative assessment, *Appl. Opt.*, *32*, 7505–7511.

Howard-Williams, C., and W. F. Vincent (1984), Optical properties of New Zealand lakes: I. Attenuation, scattering, and a comparison between downwelling and scalar irradiances, *Arch. Hydrobiol.*, *99*, 318–330.

James, M. R., W. Vant, and C. Severne (2003), Lake management requirements from a local perspective, in *Freshwater Management, Global Versus Local Perspectives*, edited by M. Kumagai and W. F. Vincent, pp. 191–216, Springer, New York.

Kirk, J. T. O. (1991), Volume scattering function, average cosines, and the underwater light field, *Limnol. Oceanogr.*, *36*, 455–467.

Kirk, J. T. O. (1994), *Light and Photosynthesis in Aquatic Ecosystems*, 509 pp., Cambridge Univ. Press, New York.

Kishino, M., M. Takahashi, N. Okami, and S. Ichimura (1985), Estimation of the spectral absorption coefficients of phytoplankton in the sea, *Bull. Mar. Sci.*, *37*, 634–642.

Kumagai, M., , and W. F. Vincent (Eds.) (2003), *Freshwater Management, Global Versus Local Perspectives*, 234 pp., Springer, New York.

Mobley, C. D. (1994), *Light and Water*, 592 pp., Elsevier, New York.

Mobley, C. D., L. K. Sundman, and E. Boss (2002), Phase function effects on oceanic light fields, *Appl. Opt.*, *41*, 1035–1050.

Morel, A. (1988), Optical modeling of the upper ocean in relation to its biogenous matter content (case I waters), *J. Geophys. Res.*, *93*, 10,749–10,768.

Morel, A., and H. Loisel (1998), Apparent optical properties of oceanic water: Dependence on the molecular scattering contribution, *Appl. Opt.*, *37*, 4765–4776.

Pegau, W. S., D. Gray, and J. R. V. Zaneveld (1997), Absorption and attenuation of visible and near-infrared light in water: Dependence on temperature and salinity, *Appl. Opt.*, *36*, 6035–6046.

Petzold, T. J. (1972), Volume scattering functions for selected ocean waters, *Ref. 72-78*, Scripps Inst. Oceanogr., La Jolla, California.

Pope, R. M., and E. S. Fry (1997), Absorption spectrum (380–700 nm) of pure water. II. Integrating cavity measurements, *Appl. Opt.*, *36*, 8710–8723.

Rae, R., C. Howard-Williams, I. Hawes, A.-M. Schwarz, and W. F. Vincent (2001), Penetration of solar ultraviolet radiation into New Zealand

lakes: Influence of dissolved organic carbon and catchment vegetation, *Limnology*, *2*, 79–89.

Roesler, C. S. (1998), Theoretical and experimental approaches to improve the accuracy of particulate absorption coefficients derived from the quantitative filter technique, *Limnol. Oceanogr.*, *43*, 1649–1660.

Roesler, C. S., and E. Boss (2003), Spectral beam attenuation coefficient retrieved from ocean color inversion, *Geophys. Res. Lett.*, *30*(9), 1468, doi:10.1029/2002GL016185.

Roesler, C. S., M. J. Perry, and K. L. Carder (1989), Modeling in situ phytoplankton absorption from total absorption spectra in productive inland marine waters, *Limnol. Oceanogr.*, *34*, 1510–1523.

Sathyendranath, S. (Ed.) (2000), *Remote Sensing of Ocean Colour in Coastal, and Other Optically-Complex, Waters, IOCCG Rep. 3*, 140 pp., Int. Ocean-Colour Coord. Group, Dartmouth, N. S., Canada.

Schindler, D. W., K. G. Beaty, E. J. Fee, D. R. Cruikshank, E. R. DeBruyn, D. L. Findlay, G. A. Linsey, J. A. Shearer, M. P. Stainton, and M. A. Turner (1990), Effects of climatic warming on lakes of the central boreal forest, *Science*, *250*, 967–970.

Seehausen, O., J. J. M. van Alphen, and F. Witte (1997), Cichlid fish diversity threatened by eutrophication that curbs sexual selection, *Science*, *277*, 1808–1811.

Smith, R. C., and K. S. Baker (1981), Optical properties of the clearest natural waters (200–800 nm), *Appl. Opt.*, *20*, 177–184.

Stramski, D., A. Sciandra, and H. Claustre (2002), Effects of temperature, nitrogen, and light limitation on the optical properties of the marine diatom *Thalassiosira pseudonana*, *Limnol. Oceanogr.*, *47*, 392–403.

Twardowski, M. S., and P. L. Donaghay (2002), Photobleaching of aquatic dissolved materials: Absorption removal, spectral alteration, and their interrelationship, *J. Geophys. Res.*, *107*(C8), 3091, doi:10.1029/1999JC000281.

Twardowski, M. S., E. Boss, J. B. Macdonald, W. S. Pegau, A. H. Barnard, and J. R. V. Zaneveld (2001), A model for estimating bulk refractive index from the optical backscattering ratio and the implications for understanding particle composition in case I and case II waters, *J. Geophys. Res.*, *106*, 14,129–14,142.

Vertucci, F. A., and G. E. Likens (1989), Spectral reflectance and water quality of Adirondack mountain region lakes, *Limnol. Oceanogr.*, *34*, 1656–1672.

Vincent, W. F. (1983), Phytoplankton production and winter mixing: Contrasting effects in two oligotrophic lakes, *J. Ecol.*, *71*, 1–20.

Vincent, W. F. (2000), Cyanobacterial dominance in the polar regions, in *The Ecology of Cyanobacteria*, edited by B. A. Whitton and M. Potts, pp. 321–340, Springer, New York.

Vincent, W. F., and D. J. Forsyth (1983), Plankton of the open water, in *Lake Taupo*, edited by D. J. Forsyth and C. Howard-Williams, pp. 85–95, Sci. Inf. Publ. Cent., Wellington, New Zealand.

Vincent, W. F., I. Laurion, and R. Pienitz (1998), Arctic and Antarctic lakes as optical indicators of global change, *Ann. Glaciol.*, *27*, 691–696.

White, E., G. Payne, S. Pickmere, and P. Woods (1986), Nutrient demand and availability related to growth among natural assemblages of phytoplankton, *N. Z. J. Mar. Freshwater Res.*, *20*, 199–208.

C. Belzile, International Arctic Research Center, University of Alaska Fairbanks, Fairbanks, AK 99775, USA. (cbelzile@iarc.uaf.edu)

I. Hawes and M. R. James, NIWA, PO Box 11-115, Hamilton, New Zealand.

C. Howard-Williams, NIWA, PO Box 8602, Christchurch, New Zealand.

M. Kumagai, Lake Biwa Research Institute, 1-10 Uchidehama, Otsu, Shiga 520-0806, Japan.

C. S. Roesler, Bigelow Laboratory for Ocean Sciences, PO Box 475, 180 McKown Point Rd, West Boothbay Harbor, ME 04575, USA.

W. F. Vincent, Département de Biologie et Centre d'Études Nordiques, Université Laval, Sainte-Foy, Québec, Canada G1K 7P4.

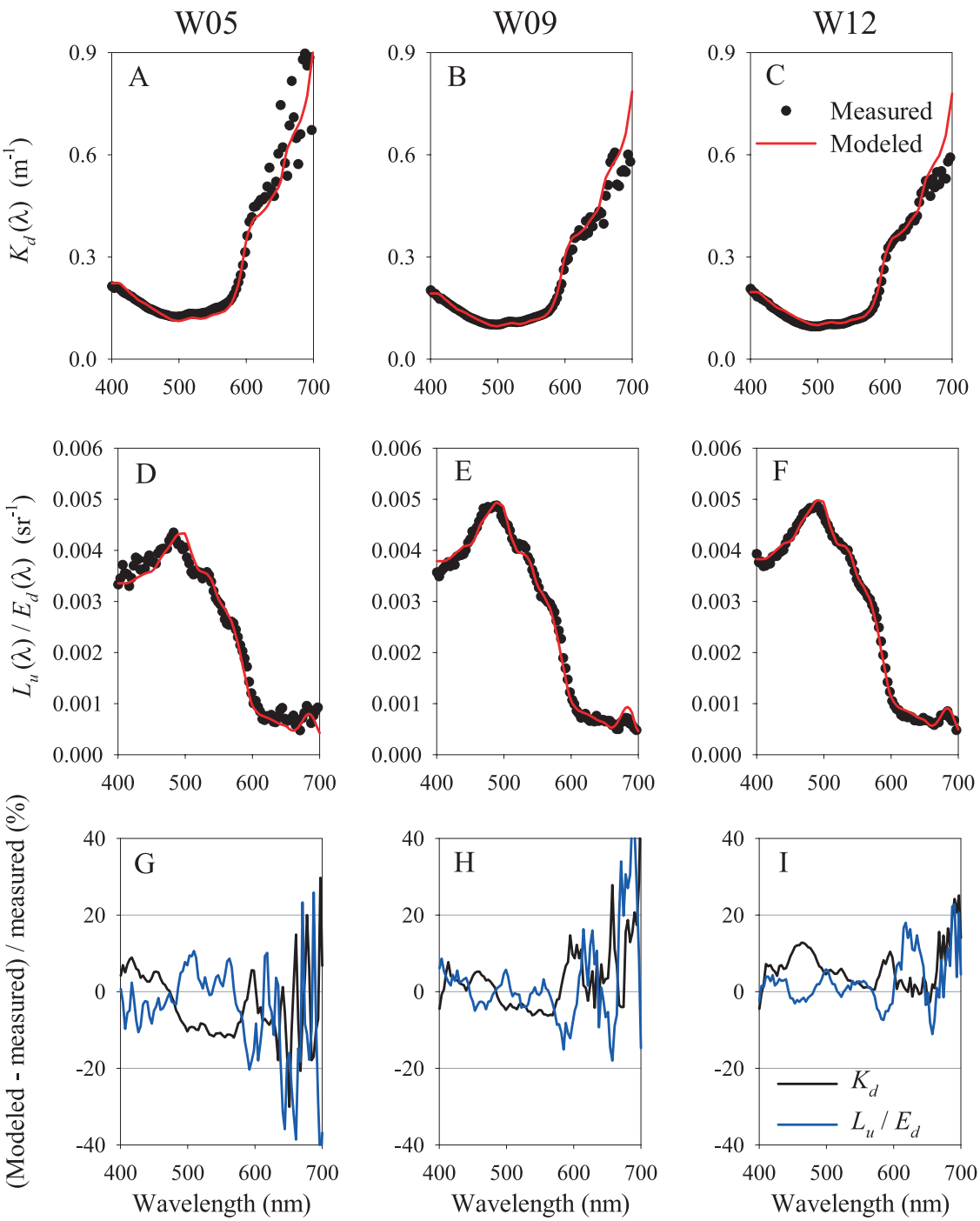

Figure 9. Measured and modeled $Kd(\lambda)$ and $L_u(\lambda)/E_d(\lambda)$ and the percent difference between modeled and measured values at three stations representing extremes in K_d, CHL*a* concentration, and atmospheric conditions. (a, d, and g) Station W05 at 16h00, clear sky, $b_{bp}/b_p = 0.008$. (b, e, and h) Station W09 at 13h00, overcast $b_{bp}/b_p = 0.010$. (c, f, and i) Station W12 at 13h00, overcast, $b_{bp}/b_p = 0.012$.